Proceedings of the Canadian Society for Mechanical Engineering International Congress
32nd Annual Conference of the Computational Fluid Dynamics Society of Canada
Canadian Society of Rheology Symposium
CSME-CFDSC-CSR 2025
May 25–28, 2025, Montréal, Québec, Canada

Modeling and Analyzing Tire-Salted Pavement Interaction Using Advanced Computational Techniques

Erin Fenton[1*], Zeinab El-Sayegh[1]
[1]Department of Automotive and Mechatronics Engineering, Ontario Tech University, Oshawa, Canada
*Erin.fenton@ontariotechu.net

Abstract—This paper introduces a novel approach for modelling the interaction between a tire and salted pavement. A passenger car tire (size 235/55R19) is modelled using Finite Element Analysis within the Pam-Crash virtual environment. The tire model is validated in both static and dynamic domains through various simulations and compared against experimental data. The salted pavement is modelled using the Smoothed Particle Hydrodynamics (SPH) technique and calibrated with a shear strength test. Tire-salted pavement interaction is simulated using a node-to-segment contact algorithm with edge treatment. The analysis focuses on tractive effort and rolling resistance under different operating conditions. This study provides insight into the interaction between tires and salted pavement, which is essential for enhancing vehicle safety, optimizing tire design, and promoting sustainable road treatment practices through advanced computational modelling.

Keywords-Tire mechanics; Rock Salt; Finite Element Analysis; Terramechanics; Tire-Salted Pavement Interaction.

I. INTRODUCTION

During winter in Ontario, Canada significant amounts of snow and ice collect on the roads creating a hazard for drivers on the road. As winter precipitation can be as high as 579 mm per season the need for additional friction on the roads is at its highest when the snow begins to melt and refreezes to the road surface. Road Salt (NaCl) is the usual solution for increasing the coefficient of friction between the tire rubber of a vehicle and the surface of the ice alongside changing the composition of the ice to increase safety [1]. With variability in driving conditions across speed and weight of the vehicles it is important to understand how tire and salt interactions can be affected.

Road salt decreases the freezing temperature of water when mixed and therefore reduces the likelihood that ice will form on roads therefore reducing the possibility for a frictionless surface to be under the vehicle tires [1]. With a decreased ability for ice to form the safety factor on the road increases significantly when drivers don't need to rely on skill alone for safety. By determining the material properties of salt in the interaction between tires, we can make roads safer for the public and understanding the resulting forces seen when salt is used on pavement. The tires within these simulations are both free-rolling and driven. A free rolling tire has a longitudinal velocity applied to it whereas a driven tire has an angular velocity applied to it representing the torque applied by the axles in a direct drive from the engine. Rock salt though widely used for snow and ice melting requires the use of its material properties for modelling.

Several studies have discussed the properties of rock salt and attempted to obtain those properties using several experimental tests. Recently in 2024, Kolano et al. [2] collected values for uniaxial compressive strength, Young's modulus, poissons ratio, tensile strength, cohesion, and internalized friction through mining and analyzing rock from the Kłodawa deposit. The study provided a detailed analysis of the geomechanical properties of rock salt from different mining fields but lacked sufficient discussion on the practical implications of the observed variability for the design. In 2018, Müller et al. [3] used discrete element modelling techniques to create polyhedral-shaped elements to represent the rock salt in 3DEC and LS-DYNA to look at microcrack growth within the material to gather anisotropic rock properties. The study presented a novel modelling strategy to study the rock salt's grain-scale fracture processes, however, it lacked a detailed discussion of broader applicability. In 2016, Chen et al. [4] used uniaxial and triaxial cyclic loading on salt cores with an RMT-150C rock mechanics testing system to determine the mechanical properties of the rock. The study provided valuable insights into rock salt's behaviour under cyclic loading but lacked clarity on the broader implications for gas storage safety and long-term stability, particularly under varying operational and environmental conditions.

Given the extensive research to obtain rock salt material properties, several researchers have modelled rock salt using advanced computational techniques. In 2023, Onyelowe et al. [5] used Smoothed Particle Hydrodynamics techniques to model clay, soil, and rock and show that SPH is best suited for geotechnical applications. The study utilized constitutive

relations and can be applied to several geotechnical engineering problems including modelling rock salt. In 2020, Zhang et al. [6] used the Backward Euler and Crank-Nicolson to model and solve shear, triaxial compression, and triaxial cycle compression of an elasto-visco-plastic that was modelled after road salt. In 2018, El-Sayegh et al.[7]used the Smoothed Particle Hydrodynamics method in Pam-Crash to model soil-tire terrain interactions resulting in vehicle performance characteristics. This study provided insight into modelling deformable bodies using a meshless free technique, however lacked experimental validation of the interaction results.

Furthermore, a significant amount of literature utilized several computational capabilities to model tire-pavement interaction and predict tire behaviour during vehicle maneuvering. In 2021, He et al. [8] used ABAQUS to model a 205/55/R16 radial tire to simulate the tire-pavement interaction during free-rolling, braking, and accelerating to study the characteristics of the contact stress at varying operating conditions. The study effectively modelled tire-pavement interaction under various conditions but lacked a detailed examination of the implications of contact stress characteristics for pavement design.

This study introduces an innovative computational approach to modelling the interaction between a passenger car tire and salted pavement, advancing vehicle safety and road treatment optimization. A detailed FEA tire model (235/55R19) is validated through static and dynamic simulations and experimental comparisons, while the salted pavement is simulated using the SPH technique calibrated with shear strength tests. The interaction is analyzed using a node-to-segment contact algorithm with edge treatment, focusing on tractive effort and rolling resistance under various conditions. By combining these advanced techniques, the study provides valuable insights into tire performance on salted roads, enabling safer tire designs, improved winter road safety, and more sustainable road treatment practices.

NOMENCLATURE

c Cohesion constant of terrain (kPa)

E Modulus of Elasticity (MPa)

Et Tangential modulus (MPa)

G Shear modulus of the terrain (MPa)

K Bulk modulus of the terrain (MPa)

k Shear deformation modulus (MPa)

ρ Density of terrain (kg/m^3)

φ Internal shear resistance (deg)

τ Shear stress (kPa)

τ_max Maximum shear stress (kPa)

σ Yield stress of the terrain (MPa)

ν Poissons ratio

II. TIRE MODELLING AND VALIDATION

A four-groove Passenger Car Radial (PCR) tire, size 235/55R19 101H, from the Continental CrossContact LX Sport model, is analyzed using Finite Element Analysis (FEA). The full tire-road interaction model was developed using Pam-Crash, a commercial finite element software, as depicted in Figure 1.

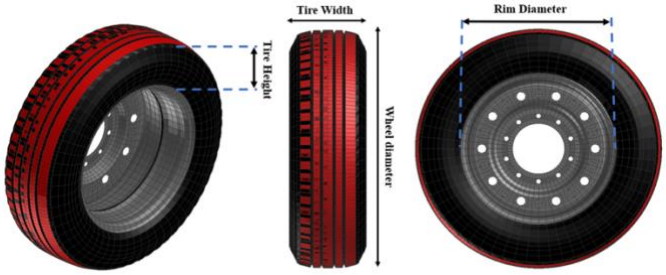

Figure 1 - Schematic of the tire model 235/55R19 Tire in Pam-Crash Software [9].

A. Material Behaviour and Modelling

To capture the hyperelastic behaviour of the tire compounds, the Mooney–Rivlin material model is employed, a widely used model in the tire industry for medium deformation scenarios. This model, derived from the Strain Energy Function (SEF) expansion proposed by Rivlin, is defined by (1) using the first and second strain invariants:

$$W = \sum_{i=0,j=0}^{\infty} C_{ij}(I_1 - 3)^i (I_2 - 3)^j \quad (1)$$

where C_{ij} are the material parameters. By retaining only, the material parameters C_1 and C_2, the Mooney–Rivlin model simplifies to (2):

$$W = C_{10}(I_1 - 3) + C_{01}(I_2 - 3) \quad (2)$$

Here, C_{01} represents the loading coefficient, and C_{10} corresponds to the unloading coefficient. Figure 2 illustrates the cross-section of the tire with labeled parts, while Table 1 provides the experimental Mooney–Rivlin material properties for the tread top and under tread.

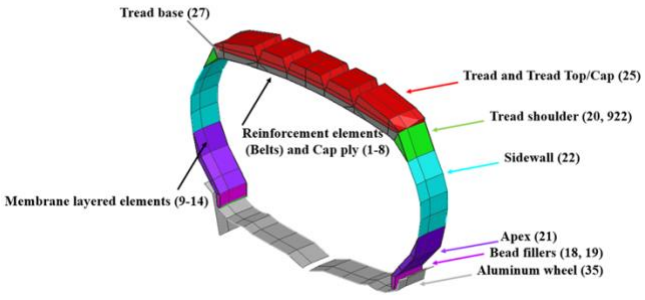

Figure 2 - Tire cross-section with different parts label [9].

Table 1- Mooney-Rivlin hyperelastic material properties for tread top and under tread [9].

Tire component	C_{01}(MPa)	C_{10} (MPa)	Poisson's Ratio
Tread	2.49	0.67	0.473
Under tread	0.51	1.86	0.409

B. Tire-Rim Assembly and Assumptions

The tire-rim assembly assumes a rigid rim with negligible tire-rim slips to simplify the simulation. The rim is modelled as a rigid aluminum alloy body, reflecting its significantly higher stiffness and mass distribution compared to the tire's layers. This assumption is consistent with typical passenger vehicle applications, where rims are designed to remain rigid during operation.

Numerical calibration was conducted for tire geometry and size parameters, including rim diameter, tire width, tire height, aspect ratio, and weight, based on data from the Continental manufacturing catalog. Table 2 compares the manufacturer's specifications with the simulated results, noting that the reported values correspond to the inflated tire state before loading.

Table 2 - Comparison between the size and weight of a 235/55R19 101H passenger car tire

Tire component	Tire geometry	Manufacture * data	Simulation results	Unit
Rim	weight	11.4	11.05	kg
	diameter	482.6	445.27	mm
Tire	weight	13.65	14.81	kg
	diameter	741.68	739.69	mm

* Manufacturer data are directly taken from the Continental website [10].

C. Static and Dynamic Validation

Tire characteristics were validated against both static and dynamic parameters, as shown in Table 3. These include vertical, lateral, and longitudinal stiffness, as well as dynamic properties such as rolling resistance, cornering stiffness, and critical vertical frequency. The validation results align with previously published data, confirming the model's reliability.

Table 3 - Tire static and dynamic FEA verification and tire manufacturer data [9]

Static	**Tire FEA verification**	**Manufacture * data**	**Simulation results**	**Unit**
	Vertical stiffness	181.1	235.86	N/mm
	Lateral stiffness	115–140	116.66	N/mm
	Longitudinal stiffness	200–250	373.11	N/mm
Dynamic	**Rolling resistance coefficient**	0.015–0.03	0.006–0.01	N/A
	Cornering stiffness	1200–1800	1057.26	N/degree
	Critical vertical frequency	70–90	74	Hz

The simulation is performed under nominal conditions of a 5 kN load and an inflation pressure of 228 kPa, ensuring consistency with the manufacturer's data and enhancing the applicability of the findings.

III. ROCK SALTED MODELLING AND CALIBRATION

To model and calibrate rock salt (NaCl) a direct shear box test was carried out using literature for the mechanical properties of salt that resulted in accurate validation of the shear-strength relationship of salt. SPH techniques were used in the shear box test that was reconstructed using a rectangular prism sized 400x200x240mm and then filled with particles that represent the salt particles, shown in Figure 3 [11].

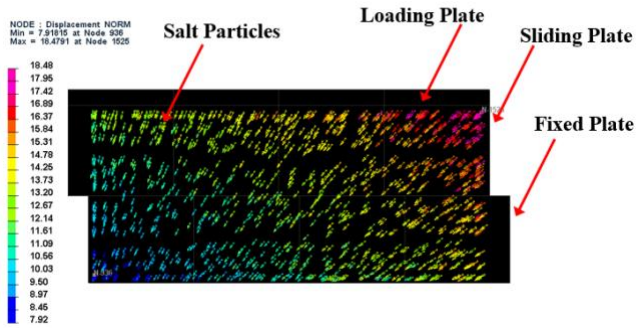

Figure 3 - Shear-Strength Test with SPH Salt

As seen the box is constructed from three parts; the fixed plate which constrains the bottom box in all directions, the sliding plate, and the loading plate which applies pressure to the particles within the box. Within this set up the box is cloned six times, and each setup incurs a different known pressure from the loading plate ranging from 0 kPa to 50 kPa with increasing increments of 10 kPa per box. Once the loading plate is loaded the sliding plate will move at a rate of 10 mm/s and will incur a final displacement of 100 mm. The shear force will continue to compute until the plate reaches the full 100mm displacement. The displacement of the nodes seen in Figure 3 allow for the visualization of the direction of travel of the rock particles during the shearing test. The resulting distance though not large shows the contrast between the original position of the rock and the final position. The largest displacement incurred by the rock salt is 18.48 mm in the upper right-hand corner. While the smallest displacement incurred by the rock salt is 7.92 mm in the bottom left-hand corner.

Within this test the SPH salt material is modelled as a Material-Type-7. Material-Type-7 is defined as an isotropic elastic-plastic hydrodynamic solid material that is named hydrodynamic elastic plastic [11]. To appropriately model this material as a road salt

there are many properties that must be inputted and calibrated in the material card, such as density (ρ), shear modulus (G), yield stress (σ), Tangent modulus (E_t), and an equation of state in (3):

$$p = c_0 + c_1\mu + c_2\mu_2 + c_3\mu_3 + (c_4 + c_5\mu + c_6\mu_2)E_i \qquad (3)$$

Using literature values that were determined through physical testing these values have been used to define the shear-strength relationship of the salt.

Table 4 - Material Properties for Rock Salt

Material Properties	**Rock Salt**
E (MPa) [12]	5.91 ± 1.20
K (MPa) [2]	7.04
G (GPa) [13]	9.34 – 11.05
c (MPa) [2]	2.12 – 5.72
σ (GPa) [14]	3
φ (deg) [2]	44 ± 0.85
$\boldsymbol{\rho}$ $(\boldsymbol{kg/m^3})$ [2]	2091.71
$\boldsymbol{\nu}$ [2]	6 ± 0.04

Using the material properties seen in Table 4, the salt particles are calibrated to obtain the best shear-strength behaviour.

The Mohr-Coulomb failure criterion shown in (4) is then used as the linear line of best fit to calibrate the shear box test behaviour in relation to the internal friction angle and cohesion that were found in the literature. As seen in Figure 4 the accuracy of the Pam-Crash validation can be seen when the internal angle of friction result is seen. According to the shear-strength relationship given in the literature, the internal angle of friction should be 44 ± 0.85 degrees whereas the results gave an internal angle of friction of 47 degrees. To further refine the results the c_1 value that is found in the material-7 card and in the equation of state (*3*) can be scaled. As seen in the literature to scale the internal angle of friction the relationship is not linear and therefore small changes must be made [11].

$$\tau_{max} = c + \sigma \tan\phi \qquad (4)$$

Where $\tau_{\max}$ represents the maximum shear strength of the salt and is plotted as a shear-strength relationship.

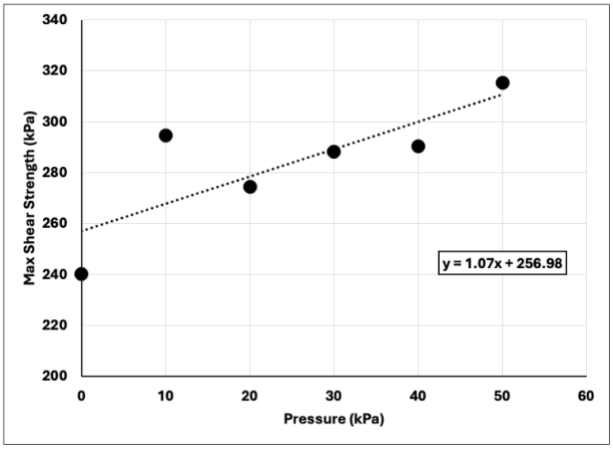

Figure 4 - Shear-Strength Relationship of Road Salt

The results in Figure 4 show the use of a linear line of best fit over the six points taken across six pressure values used to evaluate the salt using a shear box test. This test uses six values between 0 and 50 kPa the relationship between loading pressure and the shear strength of the salt can be evaluated. The trendline above can be used to determine the simulated internal friction angle and cohesion of the salt. Though the values in Table 4. are found in the literature Pam-Crash has been validated so that the results in simulation will give accurate values according to physical tests.

Based on Mohr-Coulomb failure criteria the tangent of the internal friction angle is given as the slope, and the cohesion is given as the y-intercept. In this case, the y-intercept is regarded as the cohesion is calculated as approximately 257 kPa. While the angle of internal friction is calculated using $\tan^{-1}(1.0732)$ and is approximately 47.02 degrees. This value falls close to the range seen in rock salt testing that took place in Kłodawa as seen in Table 4 [2]. The average internal friction angle is 44 ± 0.85 degrees showing that the final validated simulation was within 6% of physical testing results.

IV. TIRE-SALTED PAVEMENT ANALYSIS

In this section, the results of a loaded passenger tire interacting with a salted pavement will be presented. The passenger tire has been simulated in two ways to simulate tractive effort and rolling resistance when the tire is run over a slippery salted pavement. The pavement is simulated with a low coefficient of friction at 0.2 to emulate a road that has been covered with ice [15]. In conditions such as this road salt is used to ensure added traction and reduce the formation of ice.

The passenger tire was loaded on a low coefficient of friction surface with modelled salt layered atop the pavement, as seen in Figure 5. The tire is moving at a constant velocity of 50kph across the surface of the road for 2 seconds. To evaluate both the rolling resistance and tractive effort seen in the test the tire is loaded with the same nominal conditions such as the vertical load, inflation pressure, and road friction.

A. Tire-Salted Pavement Contact

The modelled tire on a salted pavement sits at the beginning of the road before the test begins where the road salt is modelled in white and the road in black, seen in Figure 5. The tread of the tire seen in red along with the tire sidewall touches the road and interacts with the salt particles as the tire moves along the road at a constant velocity.

To carry out the simulations, the tire was first inflated to the specified nominal inflation pressure. The tire then had a vertical load applied to the center of the rim to mimic the weight of the vehicle. The tire then settles on the salted pavement as the simulation begins. As either simulation runs a linear velocity, or angular velocity is applied to the center of the rim to induce a constant velocity. In the rolling resistance test a constant longitudinal velocity is applied to the center of the rim to induce the drag effects a free-rolling tire experiences. In the case of the traction test a constant angular velocity is applied to the center of the rim in the lateral direction to produce the effects that torque has on the tire.

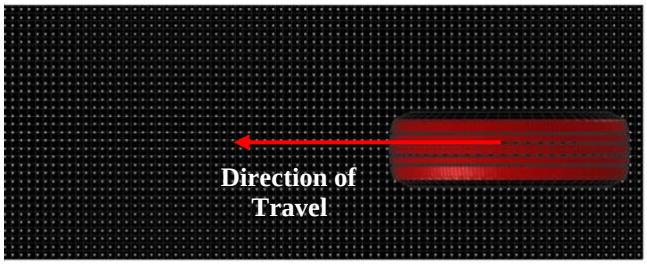

Figure 5 - Top view of tire on SPH Salted Pavement

Figure 6 shows a 5kN vertical load applied to the center of the rim and therefore creates a contact patch with the road and salt atop the pavement. As seen the road utilized is a basin with a depth of 57.92mm that holds the required density of salt without compromising the sidewalls of the tire to additional salt.

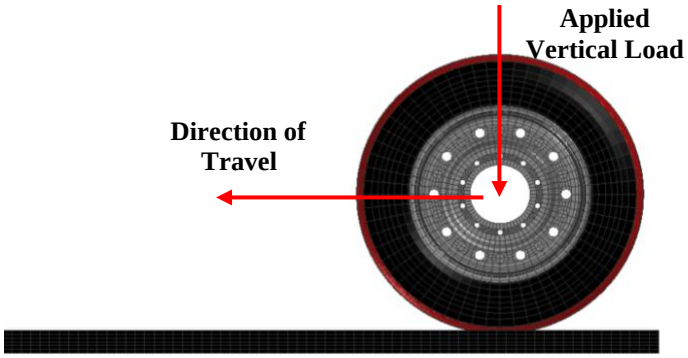

Figure 6 - Tire contact of SPH Salted Pavement

B. Traction Analysis

On a road that has a low coefficient of friction passenger tires have an increased likelihood of slipping over the surface of the pavement when ice has formed. The coefficient of friction between dry pavement and the average passenger tire is around 0.8 [15]. The coefficient of friction set in these tests is 0.2 to mimic an icy surface. The difference between the two coefficients of friction is nearly four times at which point the tractive effort of the tire will decrease.

The tractive effort of a tire is measured as these tires have a torque applied to the center of the rim. With a torque applied to the entire tire traction must be available to move the tire forward. There is increased slip with driven tires and therefore the wear will be higher than a tire that experiences the road with a linear velocity. When a free-rolling tire begins its linear motion, the tire does not have an induced torque and therefore cannot slip as it is pulled forward. The driven tire experiences a controlled amount of slip more than a free-rolling tire which increases wear. The tractive effort is defined as the ratio of the traction force to the vertical force as defined in (5):

$$TE = \frac{F_x}{F_z} \tag{5}$$

The tractive effort of the passenger tire is computed to be 0.21 on a slippery salted pavement whereas the same tire on the slippery pavement only is computed as 0.19. Thus, the salt that is added to the slippery pavement provides the driver with about 10% more traction at given operating conditions.

C. Rolling Resistance Analysis

The amount of rolling resistance in pneumatic tires changes when the road condition has been influenced by weather. With a salted slippery road, the road conditions become tricky as the road remains with a low coefficient of friction, but the road salt with a constant density works to increase the friction. The road salt influences the amount of resistance seen by the tire as the terrain is non-linear. The rolling resistance is defined as a ratio of the longitudinal force to the vertical forces on the tire and is defined as (6):

$$RRC = \frac{F_x}{F_z} \tag{6}$$

The rolling resistance of the passenger tire on a slippery salted pavement is computed to be 0.03. The rolling resistance of the same tire on a slippery pavement experiences the same rolling resistance of 0.03. In literature, a rolling resistance of 0.03 can be compared to a road surface that is made of anything between rolled gravel and an unpaved road [16]. This indicates that the road friction has minimal effect on the rolling resistance at this given condition. It must be noted that this might not be case for other operating conditions and further investigation is needed.

D. Contact Stress Analysis

Below in Figure 7a. and Figure 7b. Von-Mises stresses on the contact patch of the tire are evaluated between the tractive and rolling resistance tests, respectively.

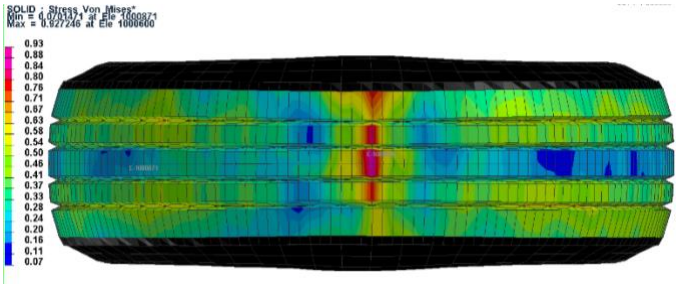

Figure 7a

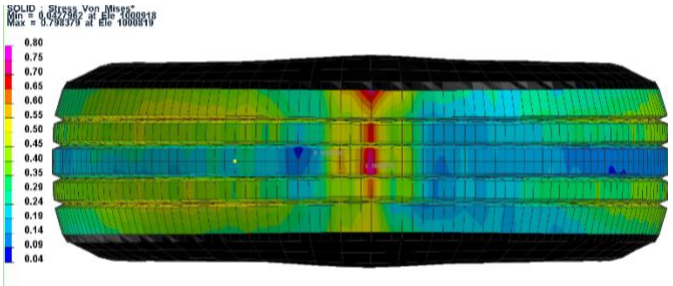

Figure 7b

Figure 7 Tire Contact Patch Von-Mises Stress a-traction test and b-free-rolling

Seen in Figure 7a. the resulting Von-Mises stress on the contact patch of the driven tire at the end of the 2-second test is 0.93 MPa. Comparatively in Figure 7b. the Von-Mises stress in the contact patch of the free-rolling tire at the end of the 2-second test is 0.80 MPa. In general, the driven tire (traction test) experienced about 16% more stress than a non-driven tire (free rolling test).

When comparing the rolling resistance test with the tractive effort test it was seen that the tractive effort test had an increase in Von-Mises stress. As the rolling resistance test does not have an applied torque to the tire there is less stress on the tread of the tire as there is no slip. The driven tire however has induced torque on a tire so increased slip is created. Slip increases the amount of friction experienced by the tire. When the tire experiences slip especially over something non-linear as salt the wear of the tire throughout the winter season increases with stress. Comparing the two Von-Mises stresses in the Figures above the highly stressed areas in the contact patch are at the same location along the tread. As the tire is loaded with the same nominal conditions between the 2 tests the contact patch remains the same the resulting stresses are however different. The driven tire has a higher stress concentration of 0.93 MPa. The free-rolling tire has a lower stress concentration of 0.80 MPa.

CONCLUSIONS

The focus of this paper is to calibrate and validate rock salt on a low coefficient of friction pavement road while looking at the influence of road salt on the tire-pavement interaction characteristics.

The rock salt modelled as SPH used parameters found in the literature. Physical measurements of salt were taken at the Kłodawa salt dome and reported in the literature [2]. As salt has a finite set of material properties the goal is to validate the physical values seen in the salt shear box test. Using a shear box test the shear-strength relationship was calculated and validated against physical metrics found in published literature. Using c_1 the results were fine-tuned to within 6% of the physical results. The resulting cohesion was calculated as 257 kPa and the internal friction angle was calculated as 44 degrees.

The results of the salt validation were used in testing the rolling resistance and tractive effort of a passenger tire across a road that was covered with salt particles. Both tests used the same nominal conditions with vertical loading and inflation pressure. The result showed the rolling resistance to be 0.03 and the tractive effort to be 0.21. The Von-Mises stress between the tire-salted pavement was evaluated at the conclusion of the 2-second run across the road. The Von-Mises stress on the tread of the driven tire was 0.93 MPa and the Von-Mises stress on the tread of the non-driven tire was 0.80 MPa.

The SPH salt model has proven to be effective in investigating the effects road salt has on passenger tires in low grip conditions of the winter season. Further research will focus on the prediction and evaluation of other tire-terrain interaction characteristics including cornering characteristics at different operating conditions.

ACKNOWLEDGMENT

The authors express their gratitude to the Natural Sciences and Engineering Research Council of Canada (NSERC Discovery Grant) for their continuous support during this research work.

REFERENCES

[1] N. Perera, B. Gharabaghi, and W. R. Trenouth, “Road salt application planning tool for winter de-icing operations,” *J Hydrol (Amst)*, vol. 524, pp. 401–410, Mar. 2015.

[2] M. Kolano, M. Cała, and A. Stopkowicz, “Mechanical Properties of Rock Salt from the Kłodawa Salt Dome—A Statistical Analysis of Geomechanical Data,” *Materials*, vol. 17, no. 14, Jul. 2024, doi: 10.3390/ma17143564.

[3] C. Müller, T. Frühwirt, D. Haase, R. Schlegel, and H. Konietzky, “Modeling Deformation and Damage of Rock Salt using the Discrete Element Method,” 2018. [Online]. Available: https://www.elsevier.com/open-access/userlicense/1.0/

[4] J. Chen, C. Du, D. Jiang, J. Fan, and Y. He, “The mechanical properties of rock salt under cyclic loading-unloading experiments,” *Geomechanics and Engineering*, vol. 10, no. 3, pp. 325–334, Mar. 2016, doi: 10.12989/gae.2016.10.3.325.

[5] K. C. Onyelowe *et al.*, “Extensive overview of soil constitutive relations and applications for geotechnical engineering problems,” Mar. 01, 2023, *Elsevier Ltd*. doi: 10.1016/j.heliyon.2023.e14465.

[6] N. Zhang and T. Nagel, “Error-controlled implicit time integration of elasto-visco-plastic constitutive models for rock salt,” *Int J Numer Anal Methods Geomech*, vol. 44, no. 8, pp. 1109–1127, Jun. 2020, doi: 10.1002/nag.3049.

[7] Z. El-Sayegh, M. El-Gindy, I. Johansson, and F. F. Fredrik¨oijer, “DETC2018/85005 OFF-ROAD SOFT TERRAIN MODELING USING SMOOTHED PARTICLE HYDRODYNAMICS TECHNIQUE,” 2018.

[8] H. He, R. Li, Q. Yang, J. Pei, and F. Guo, “Analysis of the Tire-Pavement Contact Stress Characteristics during Vehicle Maneuvering,” *KSCE Journal of Civil Engineering*, vol. 25, no. 7, pp. 2451–2463, Jul. 2021, doi: 10.1007/s12205-021-1306-0.

[9] H. Fathi, “Modeling and Analysis of All-Season Passenger Car Tire using Finite Element Analysis,” *Vehicles*, vol. 6, pp. 0–133, Feb. 2024.

[10] Continental, “CrossContact LXSport.” Accessed: Nov. 26, 2024. [Online]. Available: https://continentaltire.com/tires/crosscontact-lx-sport

[11] Z. El-Sayegh, M. El-Gindy, I. Johansson, and F. F. Fredrik¨oijer, “DETC2018/85005 OFF-ROAD SOFT TERRAIN MODELING USING SMOOTHED PARTICLE HYDRODYNAMICS TECHNIQUE,” 2018.

[12] L. Ma, Y. Wang, M. Wang, B. Xue, and L. Duan, “Mechanical properties of rock salt under combined creep and fatigue,” *International Journal of Rock Mechanics and Mining Sciences*, vol. 141, May 2021, doi: 10.1016/j.ijrmms.2021.104654.

[13] S. Shad, N. Razaghi, D. Zivar, and S. Mellat, “Mechanical behaviour of salt rocks: A geomechanical model,” *Petroleum*, vol. 9, no. 4, pp. 508–525, Dec. 2023, doi: 10.1016/j.petlm.2022.09.002.

[14] B. Reynard, R. Caracas, H. Cardon, G. Montagnac, and S. Merkel, “High-pressure yield strength of rocksalt structures using quartz Raman piezometry,” *Comptes Rendus - Geoscience*, vol. 351, no. 2–3, pp. 71–79, Feb. 2019, doi: 10.1016/j.crte.2018.02.001.

[15] S. Salimi, “Evaluation of Different Winter Road Conditions and Effectiveness of Winter Road Maintenance Operations,” Edmonton, 2014.

[16] J. Y. Wong, *Theory of Ground Vehicles*, 3rd ed. Ottawa: John Wiley & Sons, Inc., 2001.